CHAPTER 4: A TRANSMEMBRANE PORE MODEL FOR THE CX43 HEMICHANNEL BASED ON SPECTROSCOPIC MEASUREMENTS

INTRODUCTION

As detailed in the **INTRODUCTION** and previous chapters, the available Cx43 and Cx26 hemichannel models based on cryoelectron-microscopy diffraction data and image analysis show 24 transmembrane α-helical structures, but do not provide sufficient detail for helix assignment (Unger *et al*., 1999; Fleishman *et al*., 2004; Muller *et al.*, 2002; Thimm *et al.,* 205.). In Chapter 1, I presented data arguing against the notion that conserved hydrophilic residues are essential for formation of the pore (Bao *et al*., 2005). In Chapters 2 and 3, I presented SCAM data supporting the notion that M3 is a pore-lining helix, but it was not possible to assign it as helix B or C of the cryoelectron-microscopy diffraction model. The SCAM data on M1 and M2 helices were inconclusive and hence did not allow for the identification of the second pore-lining helix (Chapter 2). As mentioned in the general INTRODUCTION and in Chapter 2, the chimera and SCAM studies from other laboratories have pointed to M1 or M2 as pore-lining helices (Zhou *et al*., 1997; Pfahnl and Dahl, 1998; Hille, 2001; Skerrett *et al*., 2002; Kronengold *et al*., 2003). The limitations of these studies were discussed in Chapter 2.

In the previous chapter we discussed the methodology for the generation of hemichannels of controlled subunit composition, together with the implementation of LRET for studies of purified and reconstituted hemichannels (see Chapter 3). The advantages of using LRET for structural studies of membrane proteins in their native environment were detailed in Chapter 3 (see Fig. 3.2), and extensive studies have been performed by Bezanilla's group, as well as other investigators (Cha and Bezanilla, 1998;

Vázquez-Ibar *et al*., 2002; Knauf and Pal, 2004; Posson *et al*., 2005). Here, I present the use of LRET to measure distances between selected homologous residues in different subunit helices (same residue in different subunits) to assign the helices in the Cx43 hemichannel.

The hemichannel model based on the Cx43 gap-junctional channel electron diffraction shows the four transmembrane helices per connexin subunit, two of which line the pore: helices B and C (Fig. 4.1; Fleishman *et al*., 2004). Helix B lines the pore only near the cytoplasmic surface, where helix C diverges from the pore axis. In the model by Fleishman *et al*. (2004), M1 and M3 are proposed as the pore-forming helices, with M3 being the main pore-lining helix. However, there is no solid experimental evidence for this model and other models have been proposed from studies performed with Cx32 and Cx46, which suggest M2 or M1 as the main pore-lining helices (Skerrett *et al*., 2002; Kronengold *et al*., 2003).

As explained in Chapter 3, LRET is a technique that can provide Angstrom-resolution distances, and the analysis of the inter-helical distances from the model in Fig. 4.1 indicates that by measuring distances between the same residues in transmembrane helices of different monomers of the hemichannel (e.g., between residues at position 20 on the cytoplasmic side of M1) it will be possible to assign the helices unambiguously (see below). This will allow for the building of a model based on reliable, experimentally-determined measurements, as opposed to those derived from approaches with clear limitations (Zhou *et al*., 1997; Pfahnl and Dahl, 1998; Skerrett *et al*., 2002; Kronengold *et al*., 2003) or from phylogenetic and sequence analysis (Fleishman *et al*., 2004).

Although analysis all other inter-helical distances will help, Fig. 4.2 illustrates how measurements of distances between homologous helices in diametrically-opposed

subunits will suffice to assign the helices in the hemichannel. The distances between the centers of the helices from the model in Fig. 4.1 are shown in Fig. 4.2A. The differences in cytoplasmic distances (~15 Å) will allow for separation of helices B and C, on the one hand, from helices A and D on the other. Helices B and C may be discriminated based on the distances between the respective homologous residues near the extracellular side of the hemichannel (Fig. 4.2). Here, the shortest distance clearly belongs to helix C (26 Å) and the longest (41 Å) to helix B. Support for the assignment will also come from the degrees of tilting reflected by the differences in diametrically-opposed distances between the cytoplasmic and extracellular ends of the pore: ~11 Å for helix B and ~27 Å for helix

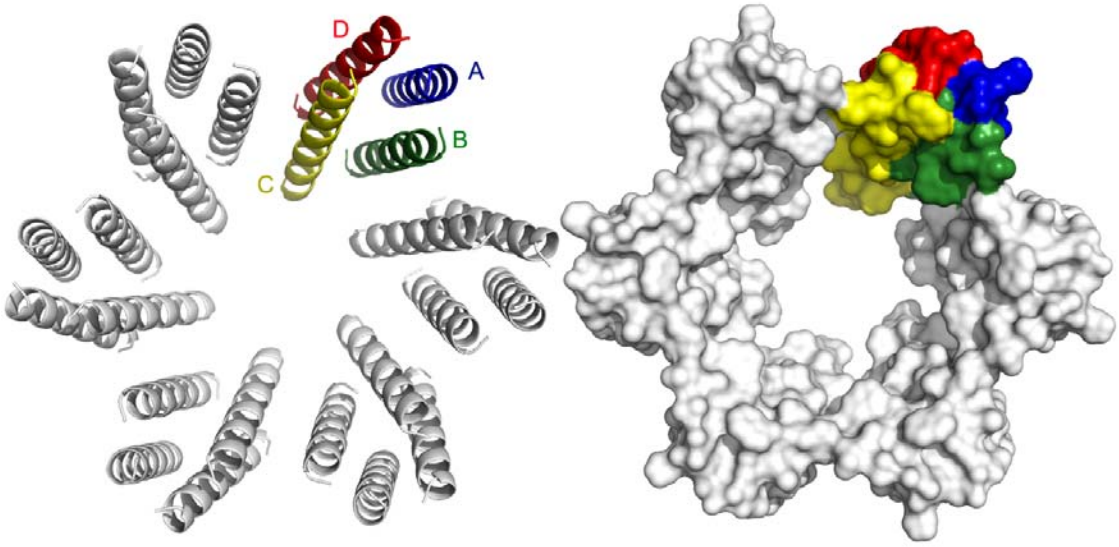

Figure 4.1: Structural model of the transmembrane hemichannel pore.

Transmembrane hemichannel pore viewed from the cytoplasmic side. The representation is based on Fleishman *et al*., 2004, and the helices are labeled A-D, as done in the original cryoelectron microscopy work from Yeager and collaborators. The helices from one monomer are denoted with colors (green, blue, yellow and red represent helices 1, 2, 3, and 4, respectively, according to the Fleishman *et al*. model). The coordinates were provided by Dr. Mark Yeager from The Scripps Institute in La Jolla, CA.

A

Table 1. Calculated lifetimes between the center of diametrically-opposed helices.

Helix pair	Extracellular distances (Å)	Lifetimes (μs)		
		R_0 = 40 Å	R_0 = 50 Å	R_0 = 65 Å
A-A	65	1,517	1,325	800
B-B	41	859	373	95
C-C	26	112	31	7
D-D	51	1,298	848	302

Helix pair	Cytoplasmic distances (Å)	Lifetimes (μs)		
		R_0 = 40 Å	R_0 = 50 Å	R_0 = 65 Å
A-A	67	1,531	1,364	873
B-B	52	1,325	894	332
C-C	53	1,350	938	363
D-D	67	1,531	1,364	873

B

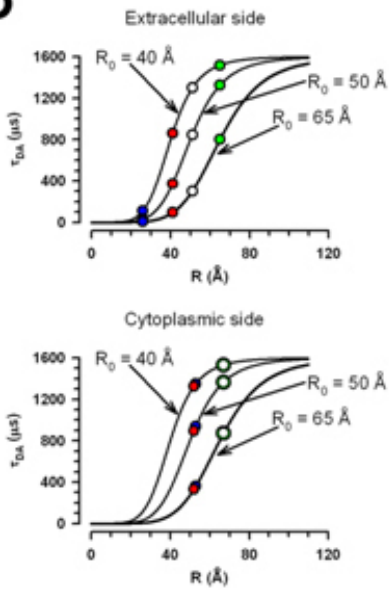

C

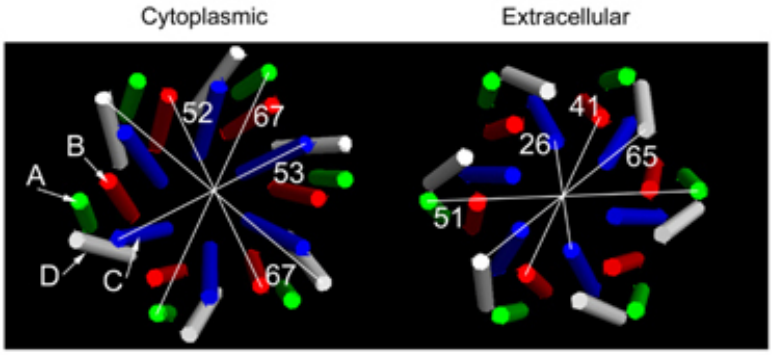

Figure 4.2: Analysis of the expected distances between the center of homologous and diametrically opposed helices of GJH based on Cx43 3D density map (coordinates provided by Dr. Yeager, from Fleishman *et al*., 2004).

A. Table showing the inter-helix distances and the expected lifetime decays in LRET experiments using donor-acceptor pairs with R_0s of 40, 50 or 65 Å. B. Graphic representation of the dependency of the lifetimes on the distance for the R_0 values above. The symbols correspond to the inter-helical distances in the table, and are color coded as described in panel C. Note that on the cytoplasmic side the white and green symbols overlap, not allowing visualization of the latter. Rates of energy transfer (E) and the lifetimes in the presence of donor and acceptor were calculated using standard energy

transfer equations (see **METHODS**), using a lifetime for Tb^{3+} of 1,600 μs. C. The helices of the six monomers that form the GJH are color coded and labeled as follows: helix A: red, helix B: green, helix C: blue and helix D: white. Views from the cytoplasmic side (left) and from the extracellular side (right). The white lines join the center of diametrically-opposed helix pairs (A-A, B-B, C-C and D-D) and the numbers denote distances in Å.

C (see Fig. 4.2). Discrimination between helices A and D should also be relatively simple, based on the degrees of tilting reflected by the differences in diametrically-opposed distances between the cytoplasmic and extracellular ends of the helices: ~2 Å for helix A and ~16 Å for helix D (see Fig. 4.2). While the distances between diametrically-opposed helices A and D are almost identical on the cytoplasmic side, there is a difference of ~15 Å on the extracellular side (shorter for helix D). The expected distance differences inferred from this analysis should translate in very significant differences in the lifetime of the sensitized emission (Fig. 4.2). In summary, LRET can provide accurate estimates of distances in the range of interest (25-80 Å), and the large predicted differences make small errors due to uncertainties related to the positions of the donor and acceptor irrelevant from the point of view of the assignment of the helices.

The approach that presented here to assign the helices is to perform experiments with purified “mixed” hemichannels that contain one monomer containing donor and one or more monomers containing acceptors (all labeled at the same position, using single-Cys mutants). As explained above, it is possible to measure the longer inter-helical distances accurately, and, this information is sufficient to assign the hemichannel helices (see Fig. 4.2).

MATERIALS AND METHODS

Choice and generation of transfer-plasmid mutants

The plan is to generate the single-Cys mutants, label them, mix them to generate hemichannels of controlled composition (e.g., one donor in one connexin monomer and one acceptor in another one), and to reconstitute them for use in the LRET experiments. In the case of M3, we employed the mutants described in Chapter 3: I156C, I157C, S158C, F161C, K162C, V164C and V167C. These include pore-lining and non pore-lining positions (see Chapters 2 and 3, and Fig. 4.4). For the distance measurements on the cytoplasmic side of the other transmembrane α helices, the following mutants were chosen: G21C and V24C (M1), L93C and A94C (M2), and N224C, I225C and I226C (M4). For the distance measurements on the extracellular side, the mutants were: G38C, T39C and A41C (M1) and F77C and V79C (M2). As mentioned in the **INTRODUCTION** of this chapter, although we can take advantage of all measurements to make the assignment, we will concentrate on the longest distances because they will show larger differences between different helices, and proved sufficient for helix assignment (see Fig. 4.2). The generation of the M3 mutants was by site-directed mutagenesis (see Chapter 3). All other mutants were produced by Mutagenex Inc. (Sommerset, NJ).

Insect cell culture, generation of baculovirus and single-Cys Cx43 mutant expression and purification

See Chapter 3 **METHODS**.

LRET experiments

The purified mutants were dephosphorylated with alkaline phosphatase as described in Chapter 3, to obtain a uniform preparation (removing the endogenous phosphorylation) of hemichannels permeable to hydrophilic solutes such as sucrose (see Chapters 3 and 5). Each purified single-Cys Cx43 mutant solubilized in 0.3% decylmaltoside was divided in three aliquots. One remained unlabeled and the others were labeled with either acceptor (fluorescein-maleimide, ATTO 465-maleimide (ATTO-maleimide), Cy3-maleimide or tetramethylrhodamine-maleimide (TMR-maleimide), or donor, Tb^{3+}-DTPA-cs124-EMCH (Tb^{3+}), by incubation for 2 h at 4^{o}C with a 10-fold molar excess of the thiol reagents. The different donor probes were chosen because of their different Förster distances (R_0) with Tb^{3+} as donor. The R_0 values are 27 Å for ATTO, 45 Å for fluorescein, 57 Å for TMR and 61 Å for Cy3-maleimide. Details about the donor Tb^{3+} probe were presented in Chapter 3. After protein labeling, the unreacted compounds were removed by gel filtration using MicroSpin G-25 columns (GE Healthcare, Piscataway, NJ). The donor-labeled, acceptor-labeled and unlabeled single-Cys Cx43 mutants were mixed in detergent at a 1:2:9 molar ratio and incubated for 2 h in the dark at room temperature, and the mixtures were reconstituted at a 1:100 protein/lipid ratio (phosphatidylcholine and phosphatidylserine, 2:1 molar ratio) by dialysis, as described in Chapter 3. From analysis of LRET data (not shown), the results in Chapter 3 and the transport assays in Chapter 5, we concluded that the average composition of the hemichannels is that of the detergent mixture, and that the actual composition follows a binomial distribution. Therefore, most hemichannels under the conditions of these experiments do not have donor subunits and the signals arise essentially from the <30 % of the hemichannels that have 1 donor subunit and 1 acceptor subunit. Because of the symmetric arrangement of the connexins in the hemichannels, there will be three donor-

acceptor distances between homologous residues in the hemichannel population: the shortest distance when the donor- and acceptor-labeled connexins are immediately adjacent, an intermediate distance when they are separated by one connexin, and a longest distance when they are separated by two connexin molecules, i.e., diametrically-opposed (Fig. 4.3).

The presence of the three distances illustrated in Fig. 4.3 will result in a multi-exponential decay that can be analyzed to obtain 2 to 3 of the distances from the lifetimes of the individual components. In practice, however, because of the different Förster distances, the longest, intermediate and shortest distance can be calculated with more accuracy from different donor-acceptor pairs. In this chapter, the data presented correspond to the "more accurate" data. In Chapter 5, "less accurate" data (smaller

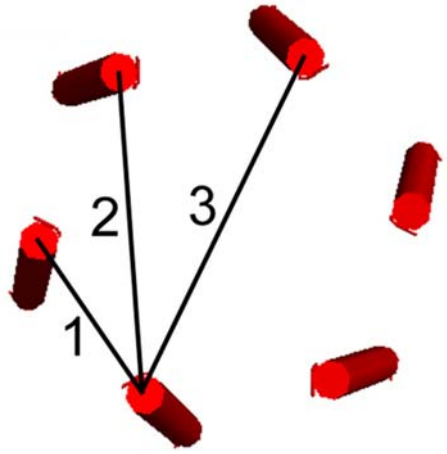

Figure 4.3: Distances between homologous α helices in diametrically opposed subunits.

Distances between helix B of monomers immediately adjacent (distance 1), separated by one monomer (distance 2) or diametrically-opposed (distance 3). Based on the coordinates of the Cx43 density map (obtained from Dr. Yeager, see Fig. 4.1 and Fleishman *et al*, 2004).

intensity decay components) are also presented. For most measurements, the emission monochromator was replaced with band-pass filters to increase light throughput. The filters from Omega Optical (Brattleboro, VT) used to record emission from the optical probes were a 520 ± 10 nm (fluorescein, ATTO 465 and ABD), a 580 ± 10 nm (TMR and Cy3) and a 590 ± 10 nm (Tb^{3+}).

Data analysis and Statistics

Single- and multi-exponential curve fitting was performed using Felix32 software, based on the analysis developed by Heyduk (2001). Fits to the data with χ^2 between 0.9 and 1.2, Durbin-Watson parameter > 1.8, and Z value > -1.96 were considered acceptable. Energy transfer (E) was calculated from the lifetimes of the donor only (τ_D) and donor and acceptor (τ_{DA}), according to: $E = 1- \tau_{DA}/\tau_D$. Distances were calculated according to: $R = R_0 \times (E^{-1}-1)^{1/6}$, where R is the distance in Å, and R_0 is the Föster distance defined earlier. For details see Heyduk and Heyduk (2001), and Selvin (2002). Data are presented as means ± SEM, and statistically significant differences were assessed by the *Student t*-test for paired or unpaired data, or one-way ANOVA, as appropriate.

RESULTS

Distances between M3 homologous residues in diagonally-opposed hemichannel subunits

The results in Chapters 2 and 3 clearly point to M3 as a pore-lining helix. For that reason, the initial LRET experiments were performed on M3 single-Cys mutants. The summary of the SCAM experiments presented in Chapters 2 and 3 is depicted in Fig. 4.4. The single-Cys mutants included the pore-lining Cys residues in I156C, I157C, F161C, V164C and V167C, and the non pore-lining Cys residues in S158C and K162C.

Examples of Tb^{3+} (donor only) and sensitized fluorescein emission decays in the I156C mutant are illustrated in Fig 4.5. The donor-only lifetimes from all the mutants of M3 (and the other helix mutants studied in this chapter) were measured and produced results undistinguishable from those in Fig. 4.5A. The sensitized emission was not polarized, as determined by emissions at 0^0 and 90^0 identical to those in solution, measured through diffusion-enhanced LRET (not shown). Figure 4.5B shows a record of the fluorescein sensitized emission for the I156C mutant. The decay can be fitted by three exponentials with lifetimes of 12, 56 and 484 μs. For the Tb^{3+}-fluorescein pair, the first lifetime is too fast to serve as a basis for a distance calculation because the calculated energy transfer is >0.99 (very close to the minimum that can be measured with the Tb^{3+}- fluorescein pair). The calculated E for the 56-μs lifetime is ~ 0.97, yielding a distance of ~26 Å, compatible with distance 2 in Fig. 4.3. As mentioned under **INTRODUCTION** in this chapter, the differences in distances between homologous helices B or C on the cytoplasmic side are very small. To obtain a reliable distance 2, however, a Tb^{3+}-acceptor pair with R_0 of 20-30 Å will be ideal (e.g., Tb^{3+}-ATTO 465, see bottom of Table 4.1). The third, slowest lifetime of 484 μs yields an energy transfer efficiency of ~0.70,

providing an accurate and reliable measure of distance 3 (~39 Å). The insert in Fig. 4.5B shows a good signal from the later portion of the sensitized emission decay. A single exponential can be fitted to this later portion of the decay, which simplifies the analysis and provides the longest distance, between homologous residues in diametrically-opposed subunits. As mentioned under **INTRODUCTION**, this distance is sufficient to assign the transmembrane pore helices of the hemichannel.

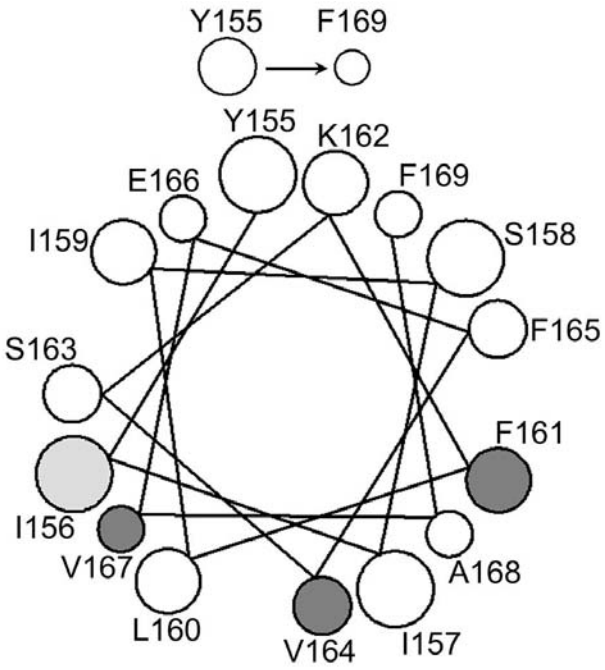

Figure 4.4: M3 helix-wheel summarizing the SCAM experiments.

The residue positions sensitive to MBB are in gray (both lighter and darker gray). The positions where IAA prevented the effect of MBB are shown in dark gray. Note that all the MBB-sensitive lie on one helix face. This Fig. is a reproduction of Fig. 2.5, shown here to simplify reading.

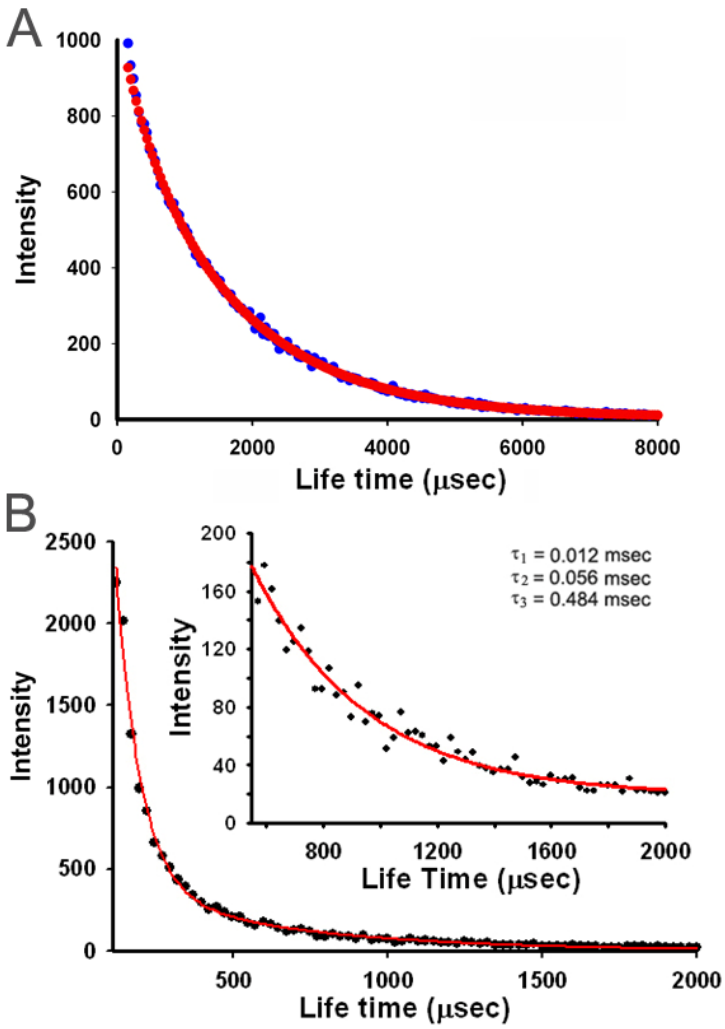

Figure 4.5: Donor-only and sensitized fluorescein emission measured in hemichannels formed by the single-Cys I156C mutant.

A. Time course of Tb^{3+} emission lifetime in hemichannels labeled only with Tb^{3+}-maleimide. The single-exponential fit to the data yielded a τ of 1,599 μs. B. Sensitized fluorescein emission. A three-exponential fitted the data better. The insert shows the later portion of the emission, starting at 600 μs, and was fit by a single exponential.

The data obtained with the Tb^{3+}-fluorescein LRET pair for the M3 single-Cys mutants studied are summarized in Table 4.1.

Table 4.1: Summary of calculated distances between homologous M3 residues in diametrically-opposed subunits

Mutant - LRET pair	lifetime (μs)	R (Å)	n
*I156C - Tb^{3+}/Fl	424 ± 19	38.9 ± 0.7	10
*I157C - Tb^{3+}/Fl	389 ± 27	37.2 ± 0.6	3
S158C - Tb^{3+}/Fl	773 ± 37	44.5 ± 0.7#	3
*F161C - Tb^{3+}/Fl	356 ± 27	36.5 ± 0.6	3
K162C - Tb^{3+}/Fl	726 ± 25	43.6 ± 0.5#	3
*V164C - Tb^{3+}/Fl	455 ± 42	39.5 ± 0.9	13
*V167C - Tb^{3+}/Fl	483 ± 39	40.1 ± 0.8	15

Mutant - LRET pair	lifetime (μs)	R (Å)	n
*I156C - Tb^{3+}/ATTO	789 ± 40	27.9 ± 0.7	10
*V167C - Tb^{3+}/ATTO	756 ± 59	27.3 ± 0.1	10

The residue positions expected to face the pore are labeled with an asterisk. The table shows the lifetimes of the sensitized emission and the calculated distances (R). Data are means ± SEM of the number of measurements shown (n). A $P < 0.05$ compared to the pore-lining positions is marked by #.

The top portion of the table shows the relevant data for the helix assignment. It is clearly apparent that the sensitized emission lifetimes, and the calculated distances, were significantly shorter for the mutants with the single Cys facing the pore (see Fig. 4.4). Therefore, these LRET data support the identification of the face of M3 that lines the pore, suggested from the SCAM results presented in Chapters 2 and 3, and Fig. 4.4. The

other important aspect of the data is that the calculated distances between 37 and 45 Å, depending on the helix face, also point to M3 as a pore-lining helix (see Fig. 4.2), again supporting the assignment based on the SCAM results. The new information obtained from the LRET data is that M3 is the "secondary" pore-lining helix, helix B, and not the "primary" pore-lining helix, helix C, as proposed by Fleisher *et al* (2004). Since helix C, but not helix B, is significantly tilted, on the narrower (extracellular) side the distances between the centers of the pore-lining helices are ~25 and 40 Å, for diametrically-opposed helices C and B, respectively. Table 1 clearly shows that the distances between homologous single-Cys in diametrically-opposed subunits closer the extracellular side of the hemichannel are not shorter than those closer to the cytoplasmic side. In fact, the data do not suggest significant tilting of M3, also supporting the assignment of M3 as helix B.

The bottom part of Table 4.1 shows data obtained from LRET between Tb^{3+} and ATTO 465. These data are entirely compatible with the distances estimated between homologous residues in next-to-neighbor subunits (distance 2 in Fig. 4.3), and the absence of tilting also supports the assignment of M3 as helix B; lack of difference in the calculated distances between residues expected to be ~3 turns of an α helix apart. A longer distance, undistinguishable from that calculated using data from the Tb^{3+}-fluorescein pair, was calculated with the Tb^{3+}-ATTO 465 pair (not shown). Additional support of the notion that the ~27 Å distance calculated from the most accurate component of the ATTO 465 sensitized emission corresponds to distance 2 of Fig. 4.3 is presented in Chapter 5.

Distances between M1, M2 and M4 homologous residues in diagonally-opposed hemichannel subunits

The main question remaining was the assignment of helix C, the primary pore-lining helix. To accomplish its identification, LRET experiments on single-Cys mutants of M1, M2 and M4 were performed. The experimental approach was the same as that described for the M3 mutants in the previous section.

Tables 4.2, 4.3 and 4.4 summarize the results from LRET data obtained on single-Cys mutants of M1, M2 and M4, respectively. The calculated distances for M1 and M4 residues were significantly longer than those for the M3 mutants in Table 4.1. The calculated distances measured for M1 single-Cys positioned near the cytoplasmic and extracellular sides of the hemichannels, and M4 single-Cys mutants positioned near the cytoplasmic side, were ~20 Å longer than those for the M3 mutants in Table 4.1. The results for the M2 mutants were dramatically different. Table 4.3 shows that for two residues located near the cytoplasmic side of the hemichannel, the distances were similar to those measured near the cytoplasmic side for the M3 mutants in Table 4.1. The results from two M2 mutants positioned near the extracellular, narrower side of the pore, show distances shorter than 25 Å. These results indicate that M1 and M4 are not pore-lining helices and that the primary pore-lining helix is M2. The assignment of M2 as helix C is based on the calculated distances and on its degree of tilting. The distances between homologous residues in diametrically-opposed helices were similar for M2 (~45 Å) and M3 (~41 Å) residues on the cytoplasmic side, but much shorter for M2 residue positions on the extracellular hemichannel side (~23 Å for M2 and ~40 Å for M3). The shorter distances between M2 residues at positions closer to the extracellular *vs*. cytoplsmic side (~ 20 Å) indicate significant tilting of M2. As discussed under **INTRODUCTION** and

illustrated in Fig. 4.2, helix C, the primary pore-lining helix, is the only pore-lining helix that displays significant tilting.

The assignment of M1 and M4 as helices A and/or D will need additional measurements with donor-acceptor probe pairs appropriate for calculations of the longer distance involved, such as those with Tb^{3+}-TMR and Tb^{3+}-Cy3 presented for cytoplasmic positions of M4 in Table 4.4.

Table 4.2: Summary of calculated distances between homologous M1 residues in diametrically-opposed subunits

Mutant - LRET pair	lifetime (μs)	R (Å)	n
G22C - Tb^{3+}/Fl	1208 ± 40	56.2 ± 1.1	15
V24C - Tb^{3+}/Fl	1265 ± 61	58.4 ± 2.0	7
G38C - Tb^{3+}/Fl	1273 ± 34	58.5 ± 1.0	18
T39C - Tb^{3+}/Fl	1005 ± 125	61.9 ± 0.8	4
A41C - Tb^{3+}/Fl	1258 ± 31	57.5 ± 1.0	8

The table shows the lifetimes of the sensitized emission and the calculated distances (R). Data are means ± SEM of the number of measurements shown (n).

Table 4.3: Inter-residual distances between diagonally-opposed M2 residues by LRET.

Mutant - LRET pair	lifetime (μs)	R (Å)	n
L93C - Tb^{3+}/Fl	979 ± 24	49.7 ± 0.5	10
A94C - Tb^{3+}/Fl	505 ± 28	40.4 ± 0.5	10

Mutant - LRET pair	lifetime (μs)	R (Å)	n
F77C - Tb^{3+}/ATTO	435 ± 17	22.9 ± 0.2	8
V79C - Tb^{3+}/ATTO	346 ± 24	23.4 ± 0.6	9

The table shows the lifetimes of the sensitized emission and the calculated distances (R). Data are means ± SEM of the number of measurements shown (n).

Table 4.4: Inter-residual distances between diagonally-opposed M4 residues by LRET.

Mutant - LRET pair	lifetime (μs)	R (Å)	n
N224C - Tb^{3+}/TMR	834 ± 35	57.9 ± 0.9	10
I225C - Tb^{3+}/TMR	870 ± 52	59.0 ± 1.4	10
I226C - Tb^{3+}/TMR	787 ± 55	57.0 ± 1.5	10

Mutant - LRET pair	lifetime (μs)	R (Å)	n
N224C - Tb^{3+}/Cy3	786 ± 87	61.1 ± 2.4	10
I225C - Tb^{3+}/Cy3	795 ± 79	61.7 ± 2.7	10
I226C - Tb^{3+}/Cy3	777 ± 50	60.5 ± 1.3	10

The table shows the lifetimes of the sensitized emission and the calculated distances (R). Data are means ± SEM of the number of measurements shown (n).

DISCUSSION

The advantages of the use of LRET for studies of membrane proteins and the experimental approach for the experiments presented in this chapter have been discussed in Chapter 3 and in the **INTRODUCTION** to this chapter. Here, I will focus on the assignment of the helices of the model presented in Fig. 4.1.

As illustrated in Fig. 4.2 and the accompanying text, there are significant differences in distances between the center of the transmembrane helices that line and do not line the pore on the cytoplasmic side of the hemichannels. The distances are ~ 15 Å longer for the non pore-forming helices A and D, compared to the pore-forming helices B and C. From the LRET data, the calculated distances allowed for the assignment of M2 (~45 Å) and M3 (~41 Å) as pore-lining helices on one hand, and M1 (~57 Å) and M4 (~60 Å) on the other hand.

The LRET data for the hemichannels between mutant positions closer to the extracellular side allowed for a clear assignment of the pore-lining helices. Of the pore-lining helices, only helix C, the primary pore-lining helix, is tilted. As a result, the expected differences in distances between the centers of homologous helices in diametrically-opposed subunits are ~ 26 and 41 Å for helices C and B, respectively. The LRET data show distances between homologous residues in diametrically-opposed subunits of ~ 23 and 40 Å, for M2 and M3 residues, respectively. The excellent agreement between the LRET calculated distances and those measured from the model in Fig. 4.1 validate the LRET measurements, and strongly suggest that the conformation of the hemichannels in the 2D crystals used in the cryoelectron-microscopy studies is similar to that of the functional hemichannels in their native environment. These data together with the evidence for tilting of M2 deduced from a shortening of distance of ~

20 Å near the extracellular side of the hemichannel, compared to the cytoplasmic side, clearly point to M2 as helix C, the primary pore-lining helix.

Regarding the non pore-lining helices M1 and M4, the data obtained so far point to M1 as helix A and M4 as helix D. The argument is the absence of significant evidence for tilting of M1. A tilting of ~15 Å is expected for helix D. However, data from M4 residues closer to the extracellular side will be needed to confirm this assignment.

Fig. 4.6 shows a hemichannel model with the assignment of the helices based on the spectroscopic LRET measurements in this chapter. This model clearly differs from those currently available, but it is the only one based on reliable experimental data, as opposed to primary sequence analysis and use of chimeras and SCAM, coupled to electrophysiological measurements (see Chapters 2 and 3).

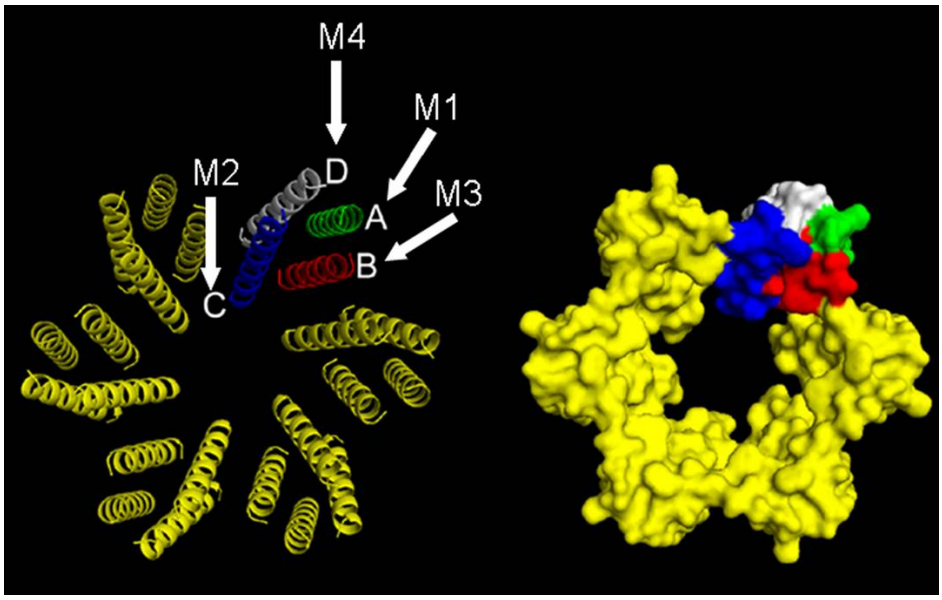

Figure 4.6: Hemichannel transmembrane pore based on the spectroscopic measurements presented in this chapter. The hemichannel is viewed from the cytoplasmic side, and the position of the helices is based on coordinates provided by Dr. M. Yeager. The pore-lining helices were assigned from the data presented in this chapter.

In summary, the data presented in this chapter allowed for assignment of the hemichannel transmembrane pore helices and resulted in the generation of a model, different from those currently available, which is based on sound spectroscopic measurements.